Supplementary Materials for

Periodic fracture behavior of nanomembrane

Yancheng Meng, Jianqiang Zhang, Baowen Li, Luxian Li, Qin Wang, Wanlin Guo

Email: wlguo@nuaa.edu.cn

This PDF file includes:

S1. Materials and Methods
PDMS film fabrication
O_2 plasma treatment
Peeling treatments
Characterization method of the cross-section

S2. Supplemental theoretical analysis
S2.1. The expression of the critical wavelength for the wrinkling instability λ_0
S2.1. A beam model for evaluating the strain in soft microfilms
S2.3. The correction of the beam model

S3. Supplemental Figures
Figure S1: Schematic illustration of the bending region of the microfilm under peeling.…
Figure S2: Schematic illustration of the correction of maximum strain in the strain profile.
Figure S3: Characterization of the $SiO_{1.8}$/PDMS bilayer film.
Figure S4: The morphology of the fold-collapse.
Figure S5: The dependence of crack depth on t_m.
Figure S6: A composite structure composed of orthogonally periodic grooves and sinusoidal wrinkles.

S4. Supplementary references

S1. Materials and Methods

PDMS film fabrications. Commercially available polydimethylsiloxane (PDMS), Sylgard 184 (Dow Corning, Midland, USA) was blended with the curing agent (catalyst) in a 10:1 mass ratio. Note, the choice of PDMS solution is crucial, preferably the original product. The mixture was cast onto a clean Si wafer and spun using a spin coater (KW-4A, SETCAS Electronics Co., China). The film thickness was controlled dependent on the time and speed of the spinning treatment. The spun mixture was degassed for 20 min in a vacuum chamber and then baked for 1 h at 80 °C in a vacuum drying oven, which was followed by curing at 35 °C overnight (10 h). The adhesion strength between the PDMS film and Si wafer was controlled by the coated layer of trichloro (1H, 1H, 2H, 2H-perfluorooctyl) silane (JKChemical, China) that was deposited on Si wafer before spinning the PDMS layer.

O_2 plasma treatments. After fabrication, the PDMS films on the Si wafer were immediately exposed to oxygen plasma in the reactor (PLAUX-PR40L from Kunshan Plaux Electronics Technology Co., Ltd. China). Treatments were performed at a pressure of 30 Pa of oxygen and a frequency of 40 kHz. The thickness of the stiff membrane ($SiO_{1.8}$) was controlled by varying irradiation time and power of the plasma treatment.

Perpendicularly peeling treatments. After plasma treatment, the sample was first chopped into strips. Then, one end of the strip was attached by tape. Finally, the strips were peeled off using a clamp (blunt-ended forceps) at a uniform speed and a bending angle of 90°. Through keeping the peeling speed, the profile of the bending region was maintained and the buckling structures were created in the bending region. As the peeling proceeds, the crease occur progressively throughout the whole bilayer until the bilayer is completely peeled off, leaving the membrane evenly fractured.

Characterization method of the cross-section. We prepared metal support in advance and transferred the bilayer film into it before the peeling. Through keeping the peeling speed, the profile of the bending region was maintained and the buckling structures were created in the bending region. Suddenly stopping the peeling treatment and fixing the end of the peeled strip, the buckling patterns can be frozen in the bending region. The front and side views of the buckling patterns were then obtained via scanning electron microscope (SEM) and confocal laser microscopy. The cross sections of the buckling patterns were milled and captured by focused ion beam technology (FIB)[S2]. The platinum (Pt) film with a thickness of about 500 nm was deposited on the target region before the milling treatment, which can make the subsequent cross-section

image smooth and burr-free. Generally, to avoid the loss of mechanical balance and new deformation near the milled region, the area of the milled region should be less than 1 μm*1 μm.

S2. Supplemental theoretical analysis

S2.1. The expression of the critical wavelength for the wrinkling instability λ_0

λ_0 can be expressed as[S4]

$$\lambda_0 = \pi \sqrt[3]{\frac{\overline{E_{\mathrm{m}}}}{3 \times \overline{E_{\mathrm{s}}}} \left(\frac{3-4\mu_{\mathrm{s}}}{(1-\mu_{\mathrm{s}})} \right)} t_{\mathrm{m}}, \tag{S6}$$

where $\overline{E}_i = E_i/(1- \mu_i^2)$ with i = m or s; μ_{m} and μ_{s} are the Poisson ratios of stiff membrane and soft microfilm, respectively; and t_{m} is the thickness of the stiff membrane. Therefore, λ_0 is proportional to the membrane thickness and independent of the thickness of soft microfilm.

S2.2. A beam model for evaluating the strain in soft microfilms

The deformation in the stiff membrane was determined by estimating the compressive strain in the soft microfilm, because the adhesion between the stiff and soft layers is strong enough to avoid delamination. Therefore, the determination of the strain in the soft microfilm is a key issue. To calculate the compressive stain in the whole bending region of the bilayer, we approximated the bending film as a cantilever beam with large deflection[S3], as shown in Fig. S1.

Ref. S3 provides a normalized expression of the large deflection of a Euler-Bernoulli cantilever beam. For convenience in following calculations, we implemented denormalization of the large deflection expression as below,

$$X(s) = L \times \cos(\phi) \left\{ \frac{s}{L} - \frac{4}{a} \left[\frac{1}{1+(\tan(\frac{\phi}{4}))^2 \exp(-2a \times \frac{s}{L})} - \frac{1}{1+(\tan(\frac{\phi}{4}))^2} \right] \right\} - L \times \sin(\phi) \frac{4}{a} \left[\frac{\tan(\frac{\phi}{4}) \exp(-a \times \frac{s}{L})}{1+(\tan(\frac{\phi}{4}))^2 \exp(-2a \times \frac{s}{L})} - \frac{\tan(\frac{\phi}{4})}{1+(\tan(\frac{\phi}{4}))^2} \right]$$

$$Y(s) = L \times \sin(\phi) \left\{ \frac{s}{L} - \frac{4}{a} \left[\frac{1}{1+(\tan(\frac{\phi}{4}))^2 \exp(-2a \times \frac{s}{L})} - \frac{1}{1+(\tan(\frac{\phi}{4}))^2} \right] \right\} + L \times \cos(\phi) \frac{4}{a} \left[\frac{\tan(\frac{\phi}{4}) \exp(-a \times \frac{s}{L})}{1+(\tan(\frac{\phi}{4}))^2 \exp(-2a \times \frac{s}{L})} - \frac{\tan(\frac{\phi}{4})}{1+(\tan(\frac{\phi}{4}))^2} \right]$$

$$\theta(s) = \phi - 4 \arctan \left[\tan(\frac{\phi}{4}) \exp(-a \frac{s}{L}) \right],$$

(S1)

where ϕ = π/2 and a is equal to $(f_0L^2/E_sI)^{1/2}$, with f_0 = 10 N/m and E_s = 1.8 MPa (the Young's modulus of the PDMS film).

S2.3. The correction of the beam model

According to the beam model, the compressive strain, $\varepsilon(s)$, on the inner surface of the bending region can be expressed as

$$\varepsilon(s) = \frac{1}{2}k(s)t_s, \tag{S2}$$

where $k(s)$ is the curvature of the bending region and can be written as

$$k(s) = \frac{8\sqrt{3}e^{-2\sqrt{3}s\sqrt{\frac{f_0}{E_s t_s^3}}}\sqrt{\frac{f_0}{E_s t_s^3}}\tan(\frac{\phi}{4})}{\left[1+e^{-4\sqrt{3}s\sqrt{\frac{f_0}{E_s t_s^3}}}\tan(\frac{\phi}{4})^2\right]}. \tag{S3}$$

The strain profile in the deflected beam can be calculated by Eqs. S1-S3 in principle. The calculations show that the strain increases with moving away from the free end and reaches a maximum at the clamped point. That is, the maximum strain appears at the clamped point (s = 0) with the maximal curvature and can be written as

$$k_{max} = k(0) = 2\sqrt{6}(\frac{f_0}{E_s})^{\frac{1}{2}}t_s^{-\frac{3}{2}}, \tag{S4}$$

$$\varepsilon_{max} = \varepsilon(0) = \frac{1}{2}k(0)t_s = \left(\frac{6f_0}{E_s}\right)^{\frac{1}{2}}t_s^{-\frac{1}{2}}. \tag{S5}$$

However, the beam model cannot correctly describe the strain distribution in the region near the clamped end since the strain must be continuous across the clamped point. In fact, the maximum strain always deviates from the clamped point, as schematically illustrated by the blue solid line in Fig. S2. The deviation lengths are determined in experiment through measuring the distance between the maximum deformation of the stiff film and the clamed point (i.e. the very peeling front), which are in a range $0.12t_s$-$0.18t_s$ and an average of $0.16t_s$. In the strain profile

calculated from the beam model, we take the value at $s = 0.16t_s$ as the maximum strain. The as-corrected maximal strain $\varepsilon(s = 0.16t_s)$ is about 0.93 times of the value at the clamped point $\varepsilon(s = 0)$, because $k(0.16t_s) = 0.93\,k(0)$.

S3. Supplemental Figures

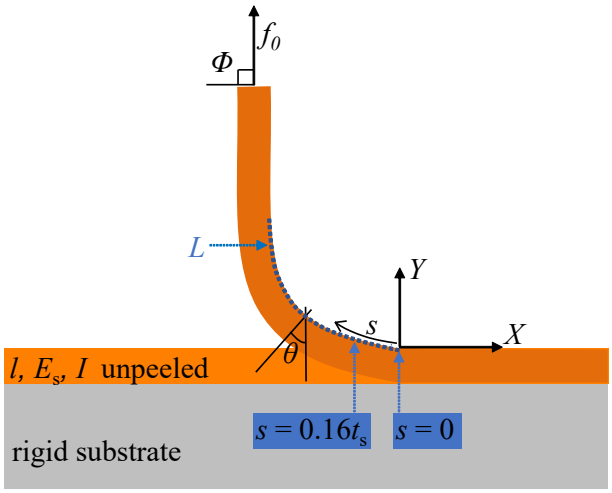

Fig. S1. Schematic illustration of the bending region of the microfilm under peeling. s and θ are the arc length and the angular deflection of the beam, respectively; ϕ is the peeling angle; X and Y are the horizontal and vertical coordinates of the bending beam, respectively. f_0 is the adhesive force per unit width between the soft microfilm and rigid substrate; L is the total length of the part with compressive strain in the whole bending region, marked with a dashed blue arc. l is the total length of the straight beam before peeling. E_s is the Young's modulus and I is the moment of inertia of the beam. $s = 0.16\ t_s$ is the deviation lengths of the maximal curvature, corresponding to maximum compressive strain, from the clamed point ($s = 0$). t_s is the thickness of the beam.

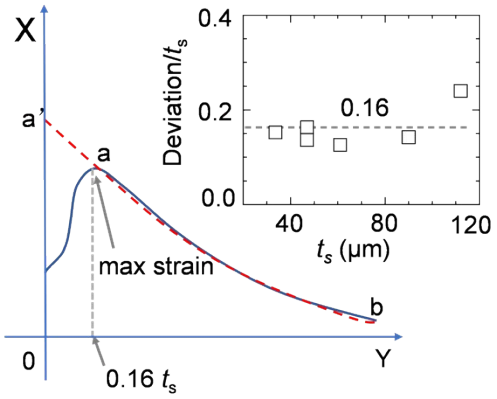

Fig. S2. Schematic illustration of the correction of maximum strain in the strain profile. Red dotted line is the strain profile of bending beam calculated by ideal beam model. Blue solid line represents practical distribution of compressive strain in the bending region. The segment of practical strain profile between "a" to "b" can be calculated and provided by an ideal beam model correctly. The practical maximum strain is at the point "a". inset, the deviation lengths between the maximum deformation of the stiff film and the clamed point, which are in a range $0.12t_s$-$0.18t_s$ and an average of $0.16t_s$.

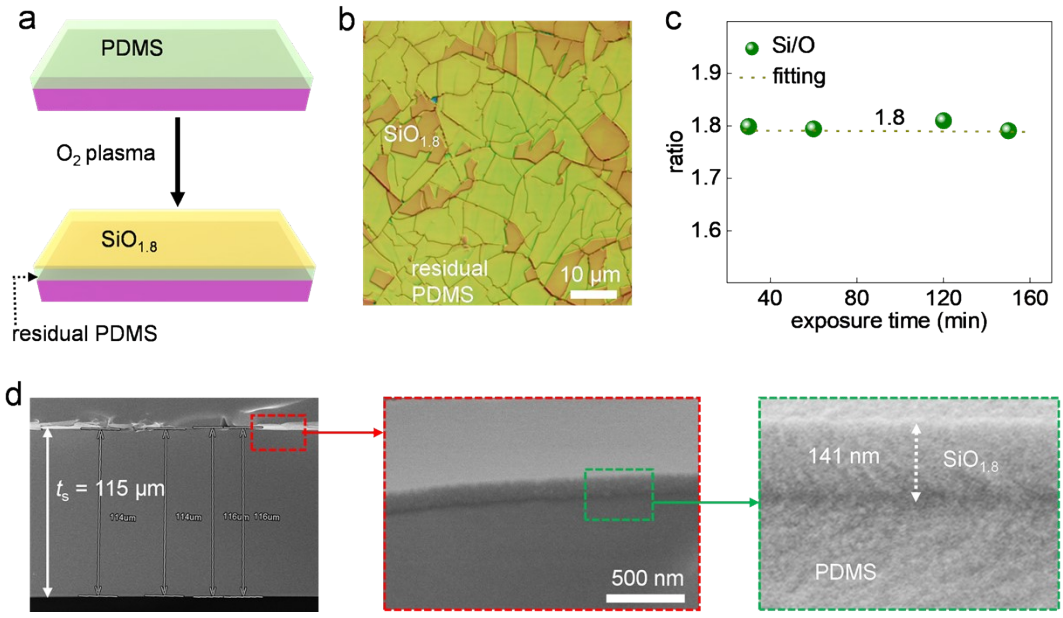

Fig. S3. Characterization of the $SiO_{1.8}$/PDMS bilayer film [S5- S6]. **a,** Schematical illustration of the preparation of $SiO_{1.8}$/PDMS bilayers. **b,** Confocal laser microscope image, illustrating the results of mechanical exfoliation of the $SiO_{1.8}$ layer from the residual PDMS substrate [S5]. The dark yellow islands correspond to the oxide layer fragments, and the large yellowish area is the bare surface of the residual PDMS layer. The plasma treatment conditions are power of 150 W and time of 40 min. **c**, XPS results, depicting atomic ratios between oxygen and silicon in oxidized surface of PDMS films after O_2 plasma treatment with different exposure times, the average atomic ratio is 1.8. **d**, Scanning electron microscopy (SEM) images, showing the cross-section of the $SiO_{1.8}$/PDMS bilayer, t_s represents the thickness of residual PDMS layer.

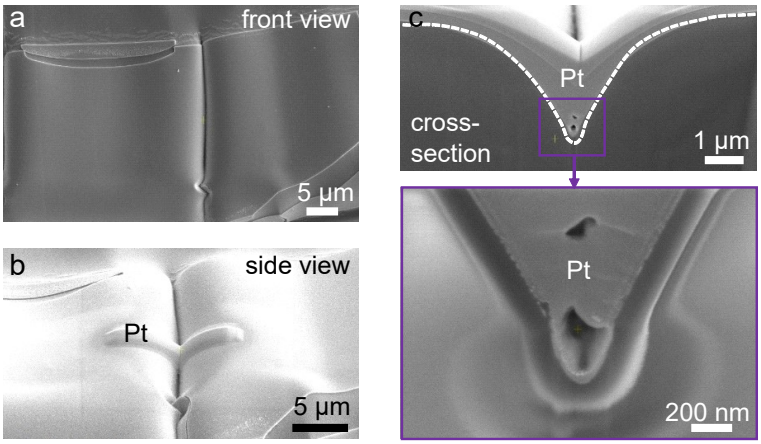

Fig. S4. The morphology of the crease. (a) SEM images, showing the front view of a crease. (b) side view of the crease. (c) FIB images, showing the cross-sections of this crease and enlarged view of its bottom, white dotted line represents the profile of the crease. "Pt" represents platinum film, needed to mill the cross-section by focused ion beam.

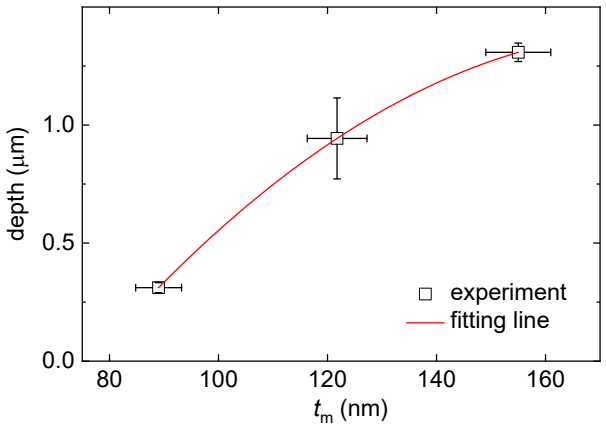

Fig. S5. The dependence of crack depth on t_m.

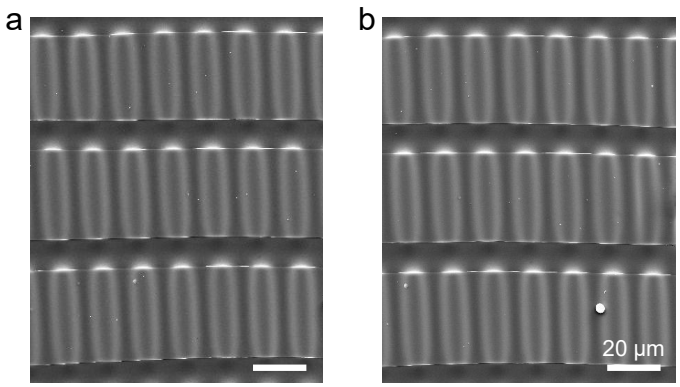

Figure S6: A composite structure composed of orthogonally periodic grooves and sinusoidal wrinkles. **a,** SEM image of the composite structure. **b,** Image of the composite structure after 20 cycling stretching.

S4. Supplemental References

S1. Meng, Y., Gong, X., Huang, Y. & Li, L. (2019). Mechanically tunable opacity effect in transparent bilayer film: Accurate interpretation and rational applications. *Appl. Mater. Today* 16, 474-481.

S2. Cairney, J. M., Munroe, P. R. & Hoffman, M. (2005). The application of focused ion beam technology to the characterization of coatings. *Surf. Coat. Tech.* 198, 165-168.

S3. Tari, H., Kinzel, G. L., Mendelsohn, D. A. (2015). Cartesian and piecewise parametric large deflection solutions of tip point loaded Euler–Bernoulli cantilever beams. *Int. J. Mech. Sci.* 100, 216-225.

S4. Zhuo, L., Zhang, Y. (2015). The mode-coupling of a stiff film/compliant substrate system in the post-buckling range. *Int. J. Solids Struct.* 53, 28-37.

S5. Meng, Y., Li, B., Li, L., Zhang, J. & Guo, W. (2022). Electron Irradiation Frozen Effect in Stiff/Soft Bilayer Films. *Adv. Mater. Interfaces* 10, 2202056.

S6. Meng, Y., Li, B., Li, L. & Zhang, J. (2022). Buckling-Pattern-Based Characterization of Stiff Membrane on Soft Film. *Adv. Eng. Mater.*, 2201547.